Cancer Cell
Article

The *ALK*^{F1174L} Mutation Potentiates the Oncogenic Activity of MYCN in Neuroblastoma

Teeara Berry,[1] William Luther,[3] Namrata Bhatnagar,[3] Yann Jamin,[2] Evon Poon,[1] Takaomi Sanda,[3] Desheng Pei,[3] Bandana Sharma,[3] Winston R. Vetharoy,[1] Albert Hallsworth,[1] Zai Ahmad,[1] Karen Barker,[1] Lisa Moreau,[3] Hannah Webber,[1] Wenchao Wang,[3] Qingsong Liu,[4] Antonio Perez-Atayde,[6] Scott Rodig,[5] Nai-Kong Cheung,[7] Florence Raynaud,[1] Bengt Hallberg,[8] Simon P. Robinson,[2] Nathanael S. Gray,[4] Andrew D.J. Pearson,[1,9] Suzanne A. Eccles,[1] Louis Chesler,[1,9,10,*] and Rani E. George[3,10,*]
[1]Divisions of Clinical Studies and Cancer Therapeutics
[2]Division of Radiotherapy and Imaging
The Institute of Cancer Research, Sutton, Surrey SM2 5NG, UK
[3]Department of Pediatric Hematology and Oncology, Dana-Farber Cancer Institute and Children's Hospital Boston
[4]Department of Cancer Biology, Dana-Farber Cancer Institute and Biological Chemistry and Molecular Pharmacology
[5]Department of Pathology, Brigham and Women's Hospital
Harvard Medical School, Boston, MA 02115, USA
[6]Department of Pathology, Children's Hospital Boston, Boston, MA 02115, USA
[7]Department of Pediatrics, Memorial Sloan-Kettering Cancer Center, New York, NY 10065, USA
[8]Department of Molecular Biology, Umeå University, Umeå, Sweden
[9]The Children and Young People's Unit, The Royal Marsden NHS Trust, Sutton, Surrey SM2 5PT, UK
[10]These authors contributed equally to this work
*Correspondence: rani_george@dfci.harvard.edu (R.E.G.), louis.chesler@icr.ac.uk (L.C.)
http://dx.doi.org/10.1016/j.ccr.2012.06.001

SUMMARY

The *ALK*^{F1174L} mutation is associated with intrinsic and acquired resistance to crizotinib and cosegregates with *MYCN* in neuroblastoma. In this study, we generated a mouse model overexpressing *ALK*^{F1174L} in the neural crest. Compared to *ALK*^{F1174L} and *MYCN* alone, co-expression of these two oncogenes led to the development of neuroblastomas with earlier onset, higher penetrance, and enhanced lethality. *ALK*^{F1174L}/*MYCN* tumors exhibited increased MYCN dosage due to ALK^{F1174L}-induced activation of the PI3K/AKT/mTOR and MAPK pathways, coupled with suppression of MYCN pro-apoptotic effects. Combined treatment with the ATP-competitive mTOR inhibitor Torin2 overcame the resistance of *ALK*^{F1174L}/*MYCN* tumors to crizotinib. Our findings demonstrate a pathogenic role for *ALK*^{F1174L} in neuroblastomas overexpressing *MYCN* and suggest a strategy for improving targeted therapy for *ALK*-positive neuroblastoma.

INTRODUCTION

Neuroblastoma, an embryonal tumor derived from the neural crest, is the most common extracranial solid tumor of childhood (National Cancer Institute, 2005). It arises from sympathetic ganglia and adrenal glands, manifesting as thoracic, paraspinous or abdominal tumors, with metastases to bone and bone marrow in high-risk cases. Despite considerable success in the treatment of favorable-biology neuroblastoma, 5-year survival rates for children with high-risk disease, which accounts for over half of all newly diagnosed cases, seldom exceed 40% (Matthay et al., 1999). A typical feature of high-risk neuroblastoma is amplification of *MYCN*, an oncogene encoding a pleiotropic nuclear phosphoprotein in the MYC family of helix-loop-helix transcription factors (Schwab et al., 1984). *MYCN* amplification is the major genetic aberration associated with aggressive tumor phenotype and poor outcome in neuroblastoma (Brodeur et al., 1984; Seeger et al., 1985). Targeted expression of *MYCN* to

Significance

The *ALK*^{F1174L} mutation has particular relevance in cancer, not only because of its role in neuroblastoma, but also because it causes resistance to crizotinib in *ALK*-rearranged tumors in general. Our murine model of high-risk neuroblastoma defined by cooperation between ALK^{F1174L} and MYCN should provide an ideal platform for further dissection of oncogenic ALK-MYCN interactions and for screening candidate agents for their ability to inhibit ALK oncoproteins and related signaling pathways. Our therapeutic strategy of combined ALK and mTOR inhibition may benefit not only neuroblastoma patients with *ALK*^{F1174L}-positive tumors who exhibit de novo resistance, but perhaps also patients with other cancers expressing crizotinib-sensitive *ALK* aberrations that acquire resistance after a favorable initial response.

the neural crest in transgenic mice causes aggressive neuroblastomas and tumorigenesis is positively correlated with *MYCN* transgene dosage or with the development of additional genetic mutations (Hansford et al., 2004; Weiss et al., 1997). Direct inhibition of MYCN has not yet been clinically successful, thus much attention is being directed to the therapeutic targeting of molecules that modulate the activities of this potent oncoprotein.

We and others have identified activating point mutations in the anaplastic lymphoma receptor tyrosine kinase gene (*ALK*) in approximately 8% of primary neuroblastomas (Chen et al., 2008; George et al., 2008; Janoueix-Lerosey et al., 2008; Mossé et al., 2008). In our study, these mutations converted IL-3-dependent Ba/F3 cells to cytokine-independent growth, led to constitutive phosphorylation of ALK and downstream signaling, and were sensitive to the small-molecule ALK inhibitor, TAE684 (George et al., 2008). Drug-induced cytotoxicity was associated with decreased phosphorylation of ALK and its downstream effectors and with the induction of apoptosis. Inhibition of ALK expression in neuroblastoma cells harboring *ALK* mutations resulted in a similar apoptotic phenotype and impaired cell proliferation. Together, these studies suggested that *ALK* mutations may afford therapeutic targets in high-risk neuroblastoma, thus leading to early phase clinical trials of crizotinib, an ALK/MET inhibitor that has been FDA approved for use in adults with *ALK*-translocated cancers (Butrynski et al., 2010; Kwak et al., 2010).

Of several somatic activating *ALK* mutations identified in neuroblastomas, one of the more common is a cytosine-to-adenine change in exon 23, resulting in a phenylalanine-to-leucine substitution at codon 1174 (F1174L) within the kinase domain (Chen et al., 2008; George et al., 2008; Janoueix-Lerosey et al., 2008; Mossé et al., 2008). This mutation appears to be more potent than the others, correlating with a higher degree of autophosphorylation and greater transforming capacity. Moreover, it is preferentially associated with *MYCN* gene amplification in neuroblastoma and defines a subset of ultra-high-risk neuroblastoma patients with distinctly poor outcome (De Brouwer et al., 2010). Finally, ALK^{F1174L} represents one of the sites of secondary kinase domain mutations in cases of *ALK*-rearranged cancers that have become resistant to crizotinib treatment (Sasaki et al., 2010). In particular, cell line and xenograft models of human neuroblastoma with ALK^{F1174L} expression are only minimally sensitive to crizotinib (Bresler et al., 2011), suggesting that effective targeting of ALK^{F1174L} will require innovative means of combating crizotinib resistance or perhaps the development of ALK inhibitors with alternative mechanisms of action.

To determine the pathogenic consequences of ALK^{F1174L}-MYCN interactions in neuroblastoma and to identify strategies that might overcome the resistance of these tumors to crizotinib, we engineered a transgenic mouse model that overexpresses both molecules in neural crest-derived cells.

RESULTS

Generation of the *Th-ALK*^{F1174} Transgenic Tumor Model

To generate mice that overexpress ALK^{F1174L} in the neural crest, we injected blastocysts from the C57BL/6J strain with a *Th-*ALK^{F1174L} construct in which human ALK^{F1174L} cDNA was ligated downstream of the rat tyrosine hydroxylase (*Th*) promoter (Banerjee et al., 1992) (Figure 1A; Figure S1A available online). *Th* is expressed in committed sympathetic precursor cells of the neural crest, and this tissue specificity has facilitated efforts to target *MYCN* overexpression to neuroectodermal cells resulting in tumors that arise in the sympathetic ganglia and adrenal gland (Weiss et al., 1997). We verified expression of the human ALK^{F1174L} protein in 293T cells, which lack endogenous expression of ALK (Figure S1B). Germline positivity for the transgene was demonstrated in multiple founders by PCR genotyping of tail DNA. Tissue-specific expression of ALK^{F1174L} and of the endogenous wild-type (WT) murine *Alk* was confirmed by RT-PCR followed by sequencing of cDNA in the cervical sympathetic ganglia and adrenal glands of 7- to 10-day-old mice (Figure 1B). In four distinct founder lines, ALK^{F1174L} was transmitted in Mendelian ratios and produced no apparent phenotype in either hemi- or homozygotes, not only in the C57BL/6J background but also in the more "tumor-permissive" 129X1/SvJ strain.

Overexpression of ALK^{F1174L} Potentiates the Oncogenic Activity of MYCN In Vivo

A meta-analysis of *ALK* mutations in human neuroblastoma suggested that ALK^{F1174L} may play a role in promoting aggressive tumors in cooperation with *MYCN* amplification (De Brouwer et al., 2010). Otherwise, evidence to support a functional interaction between MYCN and ALK^{F1174L} in vivo is lacking. We therefore investigated the effect of co-expression of ALK^{F1174L} and MYCN in neuroblastoma by crossing *Th-*ALK^{F1174L} mice with *Th-MYCN* mice (Weiss et al., 1997). Mice hemizygotic for both ALK^{F1174L} and *MYCN* exhibited high tumor penetrance with rapid lethality superior to that observed in *MYCN* hemizygotes (Figures 1C and 1D; Table 1). Of the four *Th-*ALK^{F1174L} founder lines that were crossed with *Th-MYCN* mice, the offspring of founders 2 and 4 showed complete tumor penetrance, shorter median time to tumor onset, and decreased survival at 100 days of age compared to that of *Th-MYCN* animals (Figure 1C and Table 1). An additional pattern of complete penetrance with longer latency was obtained in founder lines 1 and 3 (Figure 1D and Table 1). All subsequent experiments described in this study were performed using offspring of founders 2 and 4.

Co-expression of ALK^{F1174L} and *MYCN* (ALK^{F1174L}/*MYCN* compound hemizygotes) led to the development of large, bulky and locally invasive thoracic and abdominal masses that arose in the paraspinal ganglia or adrenals, locations typically seen in human neuroblastoma (Figure 2A). In contrast to *MYCN* tumors that generally arise as single primary tumors, the ALK^{F1174L}/*MYCN* tumors manifested as large, synchronous primary masses (Figure 2A). Focal masses on the forelimb, neck, and shoulder were seen in a minority of animals (data not shown). No evidence of macroscopic tumor spread to other organs (skin, liver, kidney, brain and lung) was detected. Tumor bearing mice exhibited normal peripheral blood counts (data not shown) and immunostaining of bone marrow cytospins for expression of the neural crest marker tyrosine hydroxylase (TH) revealed no evidence of bone marrow metastasis (Figure S2A). The tumors exhibited robust expression of ALK and MYCN at both the RNA and protein levels (Figures 2B and 2C) and also expressed

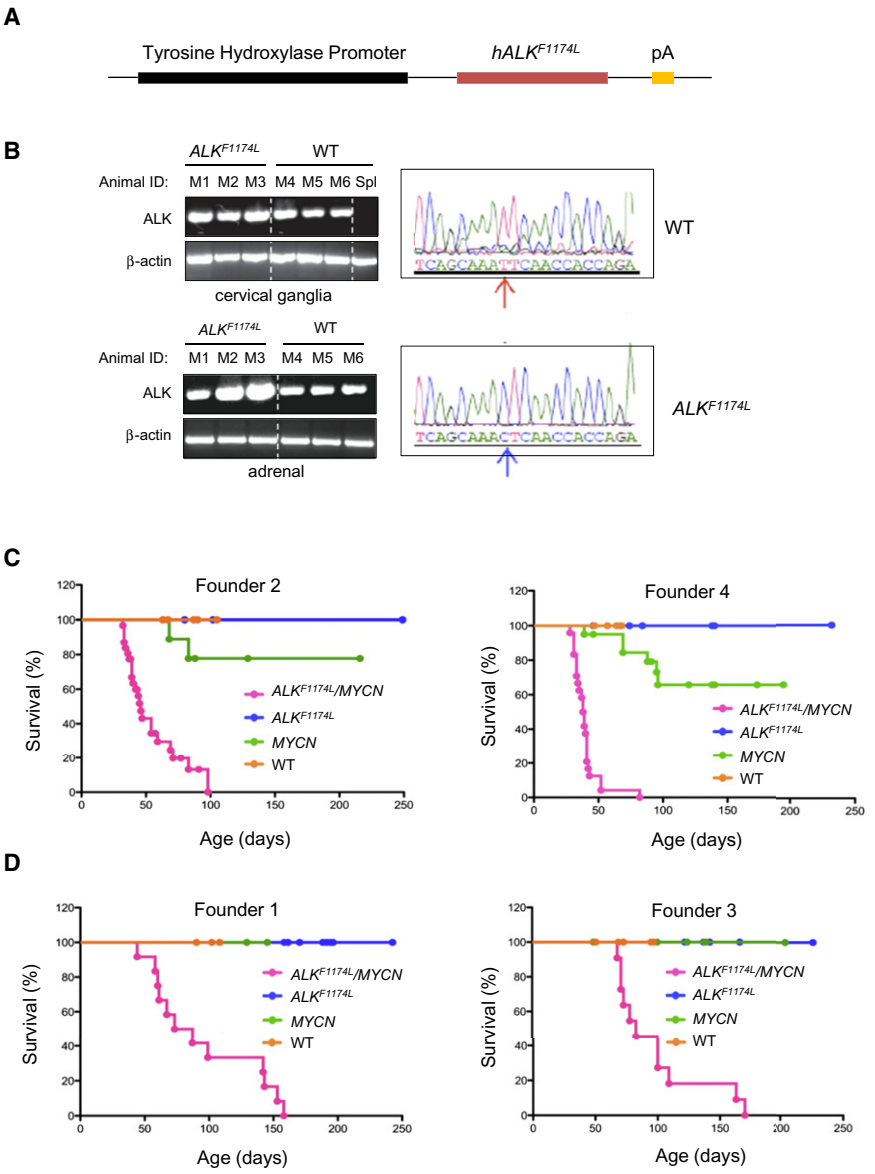

Figure 1. Overexpression of ALK^{F1174L} Potentiates the Oncogenic Activity of MYCN In Vivo

(A) The ALK^{F1174L} cDNA was ligated 3′ to the rat *Th* promoter to generate the p4.5 Th-ALK^{F1174L} transgenic construct (*Th*-ALK^{F1174L}).

(B) RT-PCR analysis of *ALK* expression in cervical ganglia and adrenal glands of 7 to 10-day-old WT mice (M4-M6) or mice transgenic for ALK^{F1174L} (M1-M3) (left panels). Spl, spleen. Electropherogram showing the change in the phenylalanine codon (TTC) in WT *ALK* to leucine (CTC) in the ALK^{F1174L} mutation in ganglia (right panel).

(C and D) Kaplan-Meier survival curves of founder lines resulting from intercrosses of *Th*-ALK^{F1174L} mice and *Th-MYCN* mice. (C) Founder 2 - ALK^{F1174L}/*MYCN*, n = 31; *MYCN*, n = 9; ALK^{F1174L}, n = 4; *WT*, n = 5. Founder 4 - ALK^{F1174L}/*MYCN*, n = 25; *MYCN*, n = 20; ALK^{F1174L}, n = 13; *WT*, n = 6. (D) Founder 1 - ALK^{F1174L}/*MYCN*, n = 12; *MYCN*, n = 6; ALK^{F1174L}, n = 12; *WT*, n = 3. Founder 3 - ALK^{F1174L}/*MYCN*, n = 11; *MYCN*, n = 10; ALK^{F1174L}, n = 11; *WT*, n = 5.

See also Figure S1.

phosphorylated ALK^{F1174L} (Figure 2C). Similar to genotypically verified human neuroblastoma tumors expressing both ALK^{F1174L} and *MYCN*, histologically, the doubly transgenic murine tumors displayed characteristic dense aggregates of poorly differentiated small round blue cells with high mitotic activity in a stroma-poor background (Figure 2D). Both human and murine tumors had similar immunohistochemical profiles of high-level cytoplasmic ALK and nuclear MYCN protein expression (Figure 2D). Positive staining for markers of human neuroblastoma, such as synaptophysin, was also evident (Figure S2B). These results demonstrate the ability of constitutively expressed ALK^{F1174L} to enhance MYCN-driven oncogenesis. Importantly, the early onset and rapid lethality of ALK^{F1174L}/*MYCN* murine tumors are characteristic of the clinical course of high-risk neuroblastoma in humans (De Brouwer et al., 2010) and thus they provide a suitable model in which to dissect ALK^{F1174L}/MYCN interactions in vivo.

ALK^{F1174L}/*MYCN* Tumors Show Differential Activation of Signal Transduction Pathways

To further characterize the aggressive nature of ALK^{F1174L}/*MYCN* tumors, we analyzed the transcriptional profiles of *MYCN*-positive tumors with or without ALK^{F1174} expression. ALK^{F1174L}/*MYCN* and *MYCN* tumors exhibited distinct genetic profiles; of the 684 genes that were differentially expressed, 476 were upregulated in ALK^{F1174L}/*MYCN* tumors (Figure 3A). Gene set enrichment analysis (GSEA) indicated significant upregulation of genes involved in the PI3K/AKT/mTOR and MAPK signal transduction pathways in ALK^{F1174L}/*MYCN* compared to *MYCN* tumors (Figure 3B), suggesting increased utilization of these two pathways in neuroblastoma cells constitutively expressing ALK^{F1174L} together with *MYCN*. This was supported by immunoblot analysis showing greater phosphorylation of AKT, as well as activation of components of the MAPK pathway, MEK and ERK, in ALK^{F1174L}/*MYCN* versus *MYCN* tumor cells (Figure 3C). These differences in activation of downstream signaling were confirmed also by immunohistochemical staining, which in addition showed upregulated mTOR activity as determined by pS6 kinase expression (Figure 3D). Similar upregulation of pS6K and pERK were seen in human ALK^{F1174L}/*MYCN*-expressing tumors compared to those with *MYCN* overexpression only (Figure 3D). Moreover, a number of kinase-associated docking proteins, such as the Src homology 2 domain-containing adaptor molecules GRB2, IRS1 and IRS2, were significantly upregulated in ALK^{F1174L}/*MYCN* tumors (Figure S3). Together, these data attest to the

Table 1. Transgenic Lines Resulting from *Th-ALK*^{F1174L} and *Th-MYCN* Intercrosses

Founder Line[a]	Genotypes	Number of Animals	Penetrance (%)	Latency (days), Median (range)
1	*Th-ALK*^{F1174L}/*MYCN*	12	100	80 (44–185)
	Th-MYCN	6	0	–
	Th-ALK^{F1174L}	12	0	–
	Th-ALK^{F1174L}/*ALK*^{F1174L}	22	0	–
	WT	3	0	–
2	*Th-ALK*^{F1174L}/*MYCN*	31	100[b]	42 (32–98)[c]
	Th-MYCN	9	25	76 (67–88)
	Th-ALK^{F1174L}	4	0	–
	Th-ALK^{F1174L}/*ALK*^{F1174L}	8	0	–
	WT	5	0	–
3	*Th-ALK*^{F1174L}/*MYCN*	11	100	83 (68–163)
	Th-MYCN	10	0	–
	Th-ALK^{F1174L}	11	0	–
	WT	5	0	–
4	*Th-ALK*^{F1174L}/*MYCN*	25	100[b]	39 (28–93)[c]
	Th-MYCN	20	35	79 (39–96)
	Th-ALK^{F1174L}	13	0	–
	Th-ALK^{F1174L}/*ALK*^{F1174L}	10	0	–
	WT	6	0	–

[a]Four *ALK*^{F1174L} founder lines exhibited neural tissue-specific overexpression of *ALK*^{F1174L} (adrenal tissue and superior cervical ganglia). *ALK*^{F1174L} (C57BL/6J) and *MYCN* (129X1/SvJ) hemizygotes were serially intercrossed into the permissive 129X1/SvJ strain. F1 *MYCN* offspring were not tumor prone, but regained 25%–35% penetrance at 100 days in F3–F4, consistent with expectations for this strain background (75%–94% 129X1/SvJ).
[b]Significantly different from penetrance in mice expressing *Th-MYCN* ($p < 0.0001$ by Student's t test).
[c]Significantly different from median (range) days to tumor onset in mice expressing *Th-MYCN* ($p < 0.0001$ by Student's t test).

predominance of these signaling networks in *ALK*^{F1174L}/*MYCN* tumors in comparison to *MYCN* tumors.

ALK^{F1174L} Enhances MYCN Protein Stabilization

Given the roles of both the PI3K/AKT/mTOR and MAPK pathways in post-translational modification of MYCN (Chesler et al., 2006; Gustafson and Weiss, 2010; Marshall et al., 2011), we determined the consequences of their activation on MYCN protein stability in the double transgenic tumors. Indeed, higher levels of MYCN were apparent in *ALK*^{F1174L}/*MYCN* versus *MYCN* tumors by immunohistochemical staining but not by immunoblotting (Figures 4A and 4D). To clarify whether *ALK*^{F1174L} expression influenced MYCN protein levels, we abrogated expression of ALK^{F1174L} in the Kelly human neuroblastoma cell line, which expresses high levels of both genes. Small interfering RNA (siRNA) knockdown of ALK^{F1174L} expression led to a decreased MYCN protein level in these cells (Figure 4B). Moreover, the half-life of MYCN protein was reduced from 90-120 min to 30 min when ALK^{F1174L} was depleted by shRNA knockdown, suggesting that ALK^{F1174L} plays a role in reducing MYCN protein turnover (Figure 4C). To determine whether MYCN stability was enhanced in *ALK*^{F1174L}/*MYCN* tumors, we analyzed the phosphorylation of serine 62 (S62) and threonine 58 (T58), which regulate MYCN protein stability (Gustafson and Weiss, 2010; Sjostrom et al., 2005). We observed decreased pMYCN^{T58} levels in *ALK*^{F1174L}/*MYCN* tumors compared to *MYCN* tumors (Figure 4D). Increased PI3K pathway activity is thought to oncogenically stabilize MYCN in neuroblastoma cells by inactivating glycogen synthase kinase 3β (GSK3β), which mediates phosphorylation of MYCN at T58 (Chesler et al., 2006; Gustafson and Weiss, 2010). The same process appears to occur in *ALK*^{F1174L}/*MYCN* tumors, where GSK3β is phosphorylated (inactivated), in contrast to *MYCN* tumors (Figure 4D). pMYCN^{T58} then binds to the E3 ligase FBXW7 and is targeted for ubiquitination and degradation (Otto et al., 2009). Using a dual-link antibody ligation assay to detect direct physical interactions between MYCN and FBXW7, we observed that knockdown of ALK^{F1174L} in Kelly cells led to increased interactions between the two proteins, further attesting to the role of this mutant in mediating decreased pMYCN^{T58} levels (Figure 4E). Thus, by promoting greater stabilization of MYCN, constitutive signaling mediated by ALK^{F1174L} appears to increase MYCN dosage in the *ALK*^{F1174L}/*MYCN* transgenic tumor model.

Upregulation of Endogenous *Mycn* RNA in *ALK*^{F1174L}/*MYCN* Tumors

A striking observation in the transcriptional signatures was the markedly increased expression of endogenous *Mycn* in *ALK*^{F1174L}/*MYCN* versus *MYCN* tumors; in fact, murine *Mycn* was among the top 25 significantly upregulated genes in our expression arrays (Figure 5A). To pursue this observation, we used qRT-PCR to measure levels of human *MYCN* and murine *Mycn* in the *ALK*^{F1174L}/*MYCN* tumors. While there was no significant difference between the levels of transgenic human *MYCN* in the two types of tumor, the expression of mouse *Mycn* RNA was indeed elevated in the *ALK*^{F1174L}/*MYCN* tumors, equivalent to expression levels of transgenic human *MYCN* (Figure 5B). There was no evidence of amplification of either oncogene on FISH analysis (Figure 5C), eliminating this mechanism as a cause of increased *Mycn* expression. To determine whether ALK^{F1174L} has a role in modulating *MYCN* expression, we measured *MYCN* mRNA levels in Kelly cells upon knockdown of ALK^{F1174L} and observed a decrease in *MYCN* mRNA levels (Figure 5D). This suggests that the constitutively activated *ALK* mutant may also regulate transcription of *MYCN*.

ALK^{F1174L} Activates an Anti-Apoptotic Program in the *ALK*^{F1174L}/*MYCN* Tumors

Ectopic expression of MYCN sensitizes cells to undergo apoptosis (Pelengaris et al., 2002). This means that efficient transformation by MYCN would require concomitant inhibition of apoptosis. Although both *ALK*^{F1174L}/*MYCN* and *MYCN* tumors exhibited similar levels of proliferation by Ki-67 staining, the amount of apoptosis as determined by TUNEL and cleaved

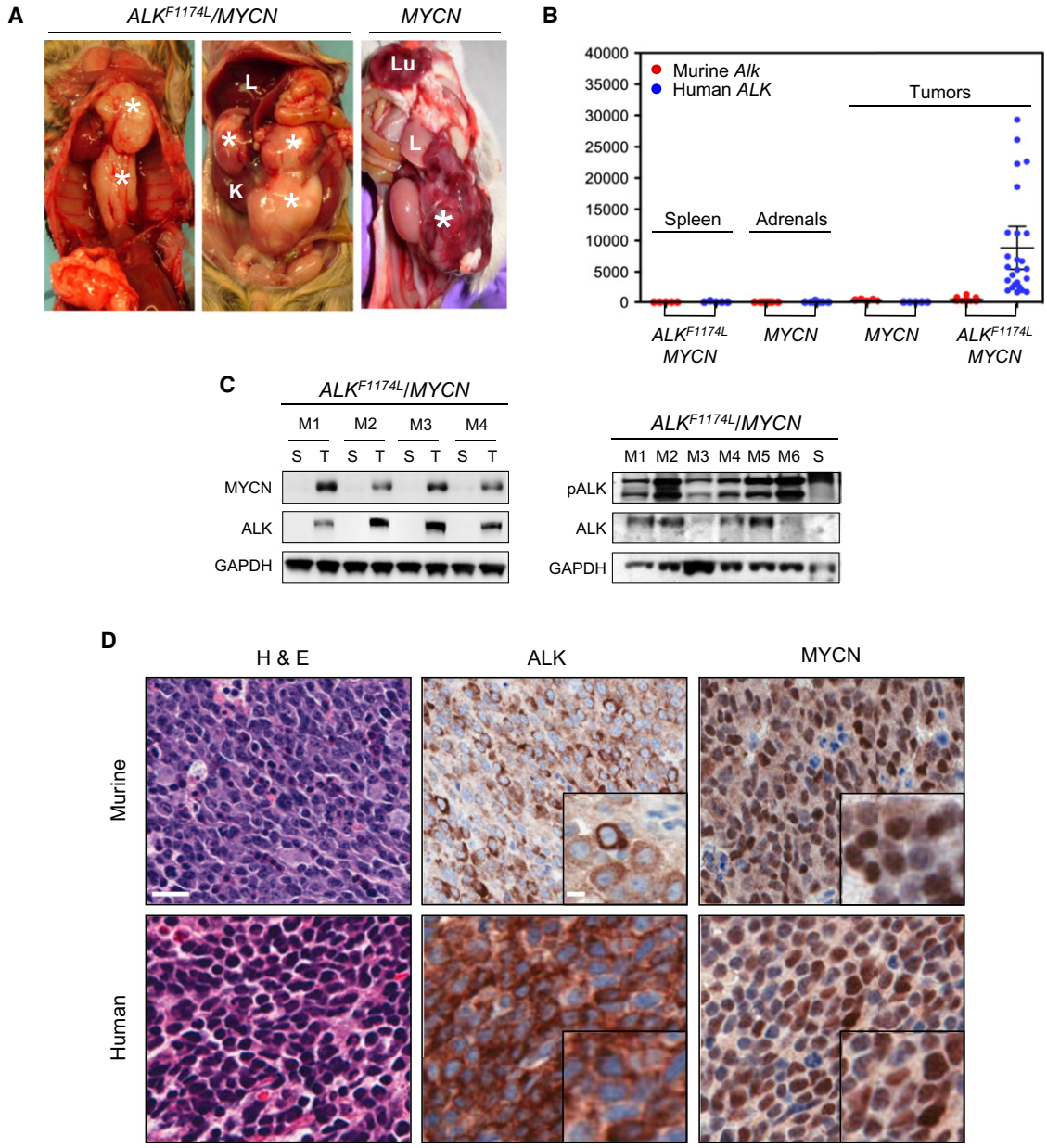

Figure 2. Combined Overexpression of *ALK*^{F1174L} and *MYCN* Results in Multifocal Neuroblastomas

(A) Gross appearance of representative *ALK*^{F1174L}/*MYCN* and *MYCN* tumors. Tumors (*) arise as multifocal primary lesions in *ALK*^{F1174L}/*MYCN* animals: thoracic paraspinous (left panel) and abdominal (right panel) tumors. K, kidney; L, liver; Lu, Lung.

(B) Quantitative RT-PCR analysis of murine and human *ALK* expression in spleen, adrenal glands and tumors from *ALK*^{F1174L}/*MYCN* or *MYCN* mice. Error bars indicate mean values ± 95% confidence interval (CI).

(C) Immunoblotting of *ALK*^{F1174L}/*MYCN* tumors (T, M1-M6) for ALK, MYCN (left panel) and pALK (right panel). pALK was detected using a human-specific ALK^{Y1604} antibody. Matched spleens (S) were used as negative controls and GAPDH was used as a loading control.

(D) H&E and immunohistochemical staining for ALK and MYCN of representative *ALK*^{F1174L}/*MYCN* murine and human neuroblastoma tumor sections. Scale bars, 20 μm, insets 5 μm.

See also Figure S2.

caspase-3 staining was greatly reduced in the *ALK*^{F1174L}/*MYCN* versus *MYCN* tumors (Figures 6A and S4). Similar differences were noted between human neuroblastoma tumors that were positive for both *ALK*^{F1174} and *MYCN* and those that were positive for *MYCN* only (Figure 6A). These findings suggest that constitutive expression of ALK^{F1174L} reduces apoptosis caused by MYCN overexpression. To test this hypothesis, we examined the gene expression profiles of these tumors, noting that expression of *Trp53* was downregulated in the *ALK*^{F1174L}/*MYCN* tumors versus *MYCN* tumors (Figure 6B). However, none of the genes

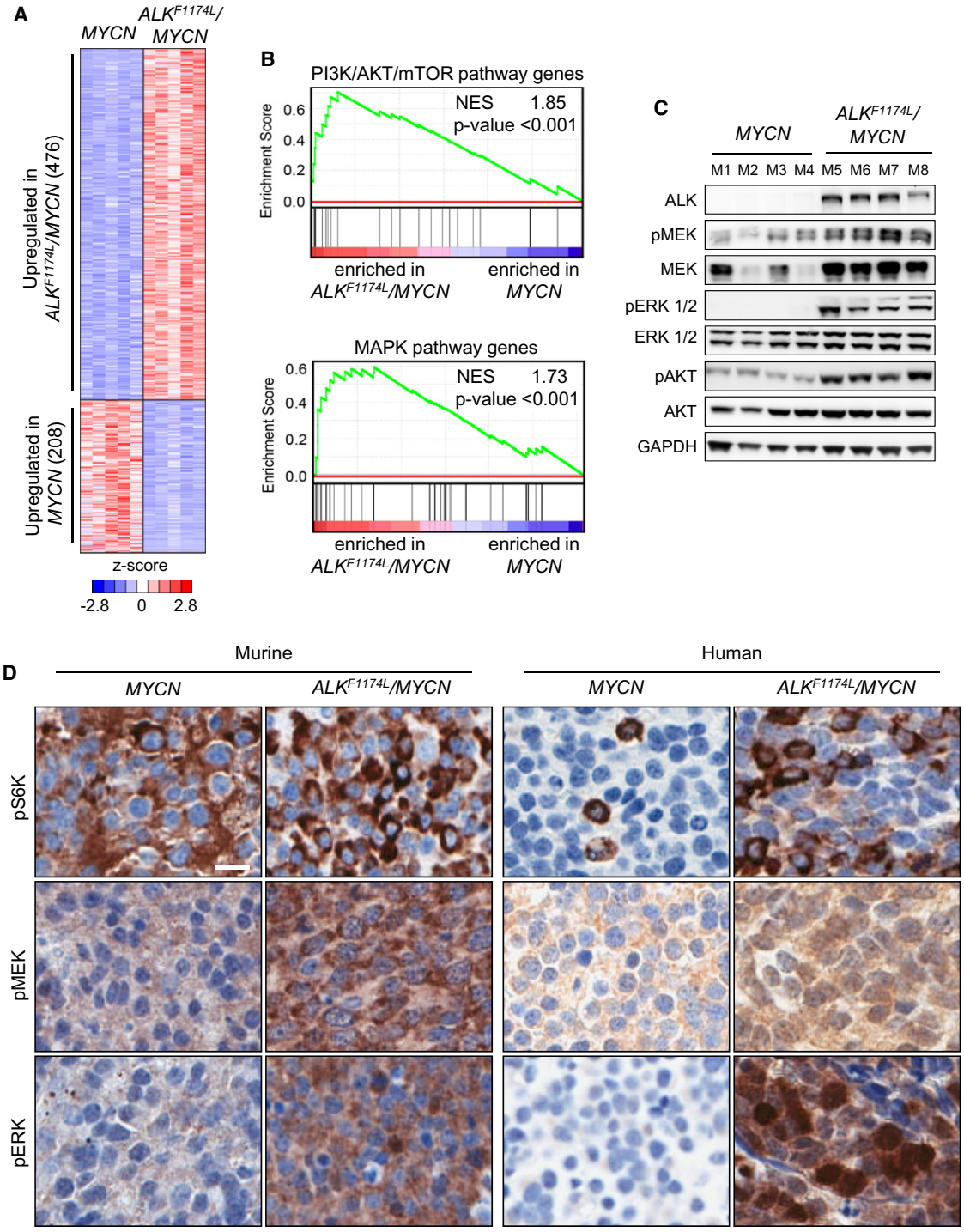

Figure 3. *ALK*^{F1174L}/*MYCN* Tumors Exhibit Distinct Expression Profiles and Downstream Signaling Compared to *MYCN* Tumors

(A) Heat map representation of differentially regulated genes in *ALK*^{F1174L}/*MYCN* versus *MYCN* tumors (fold change ≥ 2.0; corrected p value < 0.05).

(B) GSEA of PI3K/AKT/mTOR and MAPK pathway genes in transcriptional profiles of *ALK*^{F1174L}/*MYCN* and *MYCN* tumors. The normalized enrichment score (NES) and the nominal p values are indicated.

(C) Immunoblotting of PI3K/AKT/mTOR and MAPK signaling pathways in *ALK*^{F1174L}/*MYCN* and *MYCN* tumors.

(D) Immunohistochemical staining for PI3K/AKT/mTOR (pS6K) and MAPK (pMEK and pERK) pathways in *ALK*^{F1174L}/*MYCN* and *MYCN* murine and human tumors (Scale bars, 10 μm).

See also Figure S3.

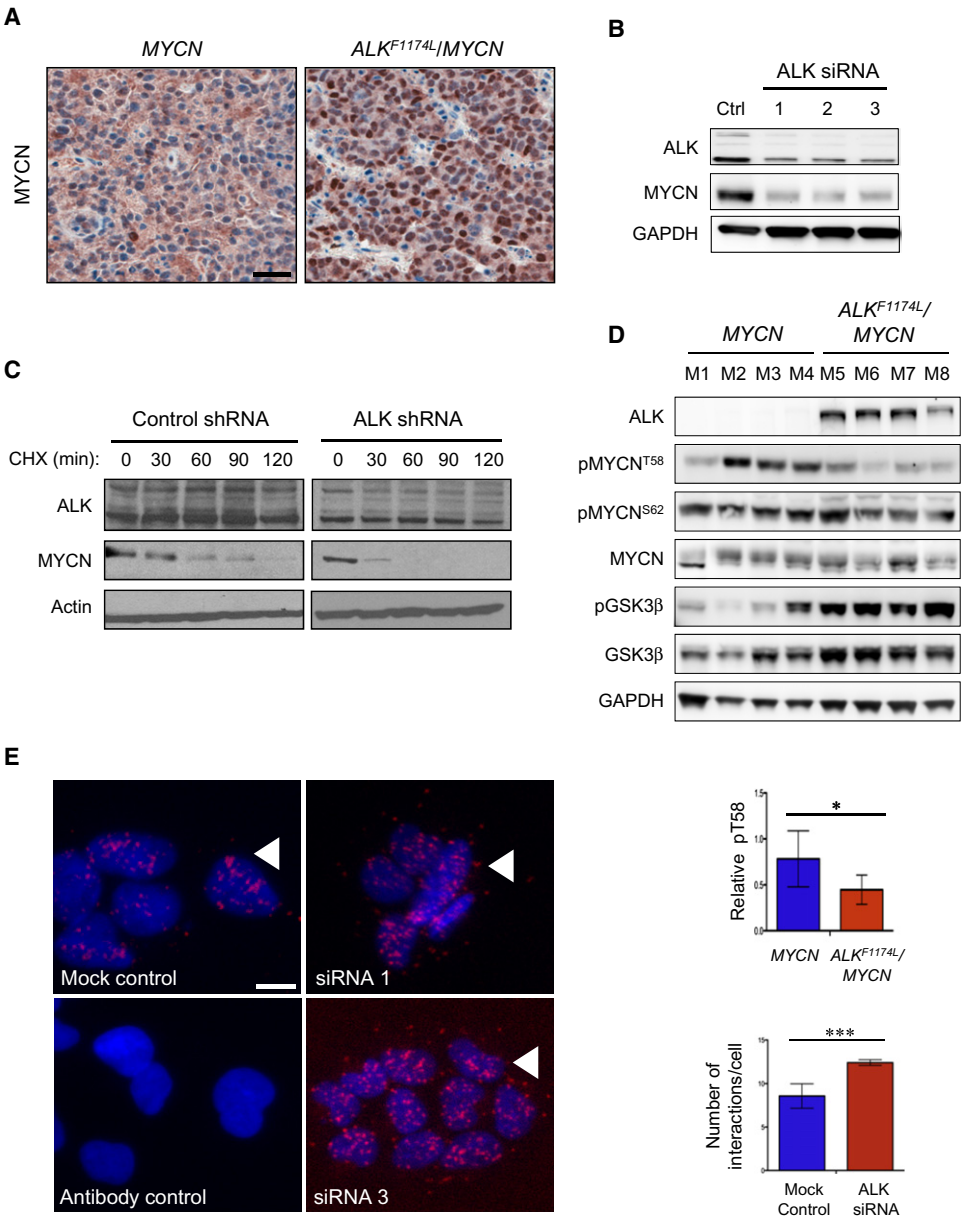

Figure 4. ALK^{F1174L} Enhances MYCN Protein Stabilization

(A) Immunohistochemical staining for MYCN in *ALK*^{F1174L}/*MYCN* and *MYCN* tumors. Scale bars, 20 μm.

(B) Western blot analysis of MYCN protein in Kelly human neuroblastoma cells after ALK^{F1174L} knockdown using three different siRNAs (1, 2, and 3). Ctl, cells expressing a control siRNA.

(C) Western blot analysis of MYCN protein expression in Kelly cells transfected with an *ALK* or control shRNA followed by treatment with 25 μmol/L of cycloheximide (CHX) and harvested at the indicated time points.

(D) Immunoblotting of *ALK*^{F1174L}/*MYCN* and *MYCN* tumors for pMYCN^{S62}, pMYCN^{T58}, and pGSK3β (upper panel). Graph (lower panel) depicts quantification of pMYCN^{T58} expression in the two types of tumors. *p = 0.05 by unpaired t test.

(E) In situ detection of MYCN:FBXW7 complex formation (arrowheads) in untreated Kelly cells (mock control), ALK^{F1174L}-depleted cells (siRNAs 1 and 3), or cells probed with secondary antibody only as a negative control (antibody control). Quantification of the number of MYCN:FBXW7 interactions in untreated Kelly cells and ALK^{F1174L}-depleted Kelly cells (right panel). Data are presented as means ± standard deviation (SD). ***p = 0.009 (Student's t test).

encoding proteins reported to be involved in MYCN-induced apoptosis that regulate p53, such as MDM2, p14^{ARF} or TWIST (Gustafson and Weiss, 2010) were differentially expressed between *ALK*^{F1174L}/*MYCN* tumors and *MYCN* tumors (data not shown). Since various BCL2 family members are direct transcriptional targets of p53 (Hemann and Lowe, 2006), we then compared the expression of BCL2 family proteins between the two tumor types. Both mRNA and protein levels of the pro-survival genes *Bcl2* and *Bclw* (*Bcl2l2*), but not *Mcl1*, were significantly upregulated in *ALK*^{F1174L}/*MYCN* tumors (Figures

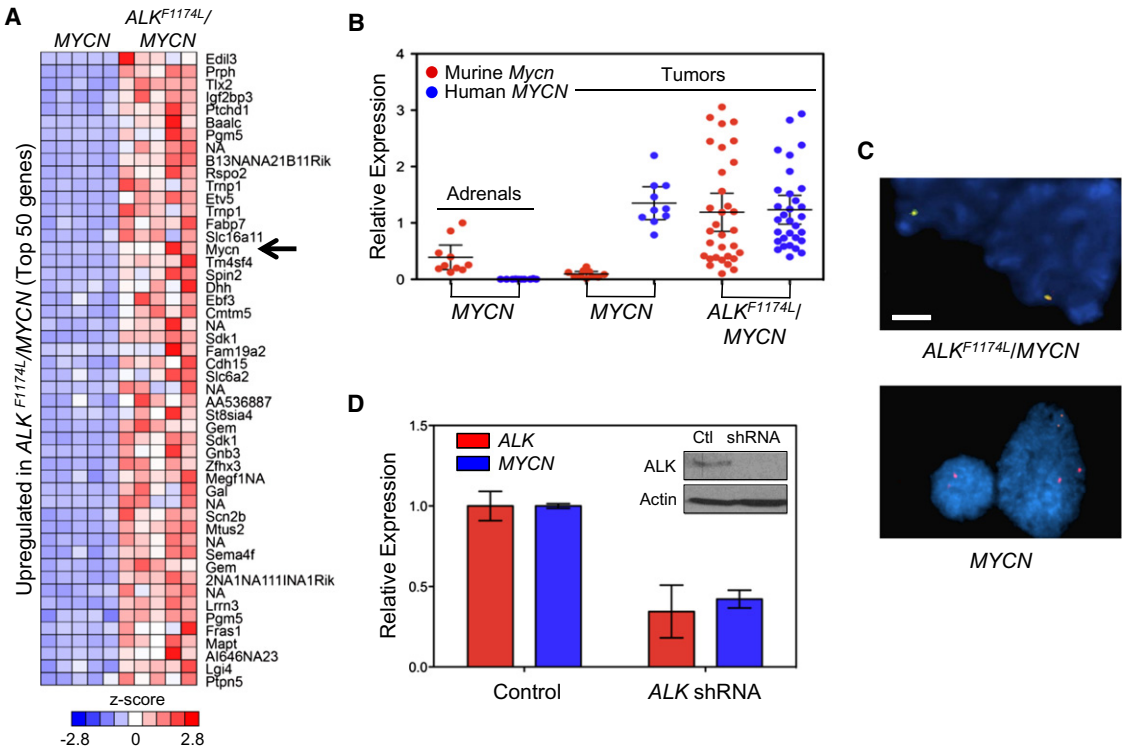

Figure 5. ALK^{F1174L} Induces Expression of Endogenous Murine MYCN

(A) Heat map representing the top 50 upregulated genes (corrected p value < 0.05, fold change ≥ 2.0) in ALK^{F1174L}/*MYCN* tumors compared with *MYCN* tumors.
(B) qRT-PCR analysis of murine and human *MYCN* expression in adrenal glands and tumors from ALK^{F1174L}/*MYCN* and *MYCN* mice. Expression is relative to either murine or human *MYCN* levels in tumors from *MYCN* heterozygotic mice. Mean values ± 95% CI are indicated.
(C) FISH analysis of murine ALK^{F1174L}/*MYCN* tumors using an *ALK* dual-color break-apart probe (upper panel) and a *MYCN* probe (lower panel) (Scale bar, 10 μm).
(D) qRT-PCR analysis of ALK^{F1174L} and *MYCN* expression in Kelly cells in which ALK^{F1174L} expression was depleted using shRNA, compared with cells in which a control shRNA was used. Western blot showing level of ALK^{F1174L} knockdown (inset). Mean ± SEM values for three independent experiments are shown. Ctl, cells expressing a control shRNA.

6B–6D). The pro-apoptotic genes *Bak* and *Bax*, the latter being a key intermediate of MYC-driven apoptosis (Hemann and Lowe, 2006), and the BH3 pro-apoptotic genes *Bik*, *Bid*, and *Noxa* were downregulated in the ALK^{F1174L}/*MYCN* tumors (Figures 6B and 6C). Together, these findings suggest that constitutively expressed ALK^{F1174L} contributes to MYCN-driven neuroblastoma by exerting an anti-apoptotic effect that allows transformed cells to evade MYCN-induced apoptosis.

Combined Inhibition of ALK^{F1174L} and Its Downstream Signaling Pathways Leads to Regression of ALK^{F1174L}/*MYCN* Tumors

Human neuroblastoma cells and xenograft models expressing ALK^{F1174L} are resistant to crizotinib (Bresler et al., 2011). To determine if such resistance was reiterated in our neuroblastoma model, we treated mice bearing ALK^{F1174L}/*MYCN* tumors with crizotinib. After documenting baseline tumor burden by serial MRIs, we treated the animals for 7 days with oral vehicle or crizotinib at a daily dose of 100 mg/kg, which has been used in xenograft models of neuroblastoma (Bresler et al., 2011). Despite partial dephosphorylation of ALK, crizotinib treatment did not appear to have an effect on tumor size (Figures 7A–7C). Histologic analysis confirmed the lack of any significant treatment effect on cellularity, while cleaved caspase-3 staining revealed no evidence of apoptosis (Figure 7D). Thus, our doubly transgenic model recapitulates the crizotinib resistance of human neuroblastoma and ALK-rearranged cancers.

Preclinical studies of crizotinib have shown that both pAKT and pERK are incompletely inhibited with doses of crizotinib that abolish ALK phosphorylation in NPM-ALK-positive lymphoma cells (Christensen et al., 2007). To determine whether the lack of response to crizotinib in the ALK^{F1174L}/*MYCN* tumors could be due to persistent or even paradoxical activation of the signaling pathways utilized by these two interacting oncoproteins, we analyzed the downstream effectors of the PI3K/AKT/mTOR and MAPK pathways. Although treatment with crizotinib led to a minimal decrease in AKT phosphorylation compared with results for vehicle-treated animals, it lacked any discernible effects on mTOR and MAPK signaling, as indicated by the persistent activation of pS6K and p4E-BP1 and of pMEK and pERK, respectively, on both western analysis and immunohistochemistry (Figures 7C and 7D).

We therefore sought to determine if these tumors could be rendered sensitive to crizotinib by adding Torin2, an ATP-competitive inhibitor of mTOR (Liu et al., 2011), a combination that had exhibited efficacy in vitro (A. Azarova and R.E.G., unpublished data). When given alone, Torin2 ablated *MYCN* tumors with reduction in MYCN protein levels and induction of

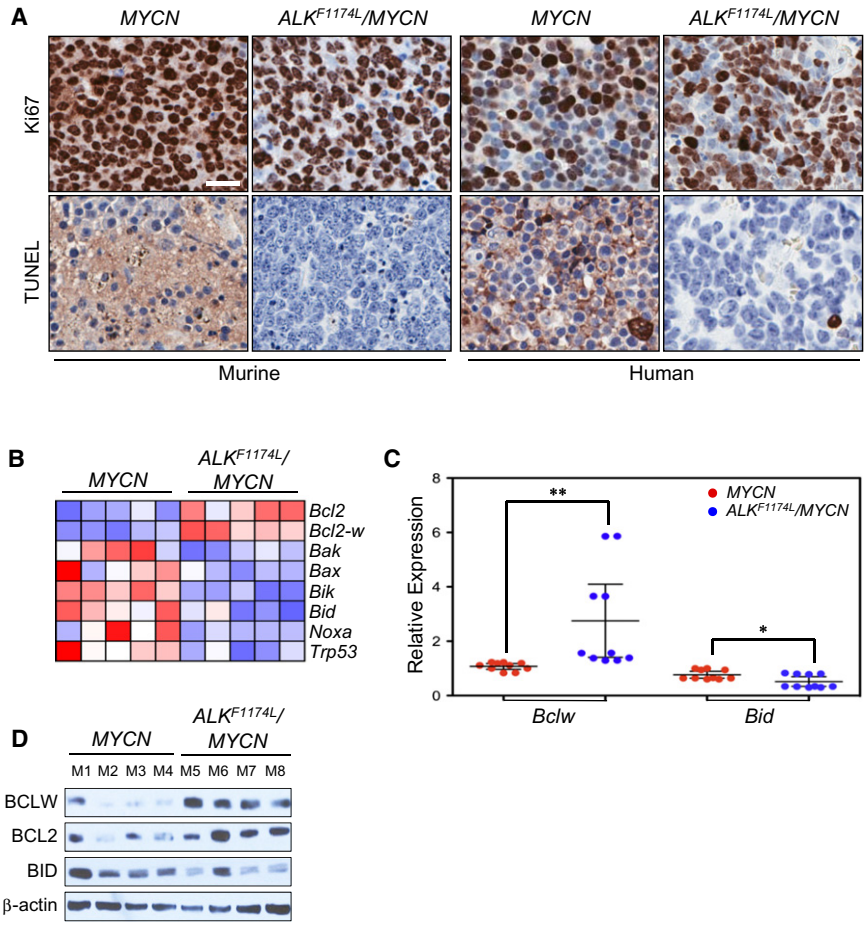

Figure 6. *ALK*^{F1174L} Promotes Anti-Apoptotic Activity in *ALK*^{F1174L}/*MYCN* Neuroblastomas

(A) Immunohistochemical staining for Ki67 and TUNEL of transgenic murine and human *ALK*^{F1174L}/*MYCN* and *MYCN* neuroblastomas. Scale bars, 20 μm.

(B) Heat map representation of the expression levels of pro-survival genes, *Bcl2* and *Bclw*, and the pro-apoptotic genes *Bak*, *Bax*, *Bik*, *Bid*, *Noxa*, and *Trp53*, in *ALK*^{F1174L}/*MYCN* and *MYCN* tumors.

(C) qRT-PCR analysis of *Bclw* and *Bid* expression in *ALK*^{F1174L}/*MYCN* and *MYCN* tumors (n = 10 in each group). Gene expression is relative to that in a *MYCN* tumor. Data are presented as mean ± SEM (*p = 0.03, **p = 0.005).

(D) Immunoblotting of *ALK*^{F1174L}/*MYCN* and *MYCN* tumors depicting expression of BCLW, BCL2, and BID proteins in the *ALK*^{F1174L}/*MYCN* and *MYCN* tumors.

See also Figure S4.

apoptosis (Figures S5A–S5C). However, concomitant expression of ALK^{F1174L} abrogated any efficacy of Torin2, as indicated by essentially stable tumor volumes after 7 days of treatment with this agent at 20 mg/kg/day (Figures 7A and 7B). Predictably, Torin2 treatment of *ALK*^{F1174L}/*MYCN* tumors in large part led to downregulation of the mTORC1 targets, pS6K and p4E-BP1, but did not affect pMEK or pERK, or induce any substantial increase in apoptosis (Figures 7C and 7D). By contrast, combined use of crizotinib (100 mg/kg/day) with Torin2 (20 mg/kg/day) for 7 days significantly reduced tumor size and growth (Figures 7A and 7B). Of the four mice receiving both agents, three had obvious regressions of their tumors, while one showed growth inhibition. The proportion of mice with tumor regression improved to 100% in a subsequent study in which 80% dosage of each drug was given in combination (data not shown). These favorable responses to combination treatment correlated with inhibition of pALK, pAKT, mTOR, and MAPK targets (Figures 7C and 7D). Importantly, the combination also led to a striking increase in apoptosis as determined by cleaved caspase-3 staining (Figure 7D). Since phospho-ALK immunoblotting does not appear to provide a reliable assessment of ALK inhibition, we confirmed by mass spectroscopy that crizotinib was present in tumor tissue at exposure levels in excess of its published IC_{50} for ALK inhibition (Bresler et al., 2011; Schönherr et al., 2012) (Table S1). The variability in total ALK levels on immunoblots of tumors treated with the combination (Figure 7C) likely reflects the significant levels of cell death observed at 7 days post-treatment (Figure 7D, H&E stain), and is not a primary effect of the therapy on ALK levels. Consistent with this possibility, immunohistochemical staining of these tumors showed large regions that stained negatively for ALK (Figure S5D), and in tumors harvested after short-term (3-day) therapy trials, uniform levels of total ALK were seen on immunoblots (Figure S5E).

We next analyzed longer-term survival using a larger number of mice (n = 10 per group) treated for 14 days. Treatment with crizotinib and Torin2 significantly prolonged survival compared to the outcome with use of vehicle or either single agent alone (Figure 7E). Indeed, all mice given the combination remained alive for 10–23 days post-treatment, whereas mice treated with crizotinib and Torin2 as single agents began to die before treatment was stopped, with none surviving for more than 10 days post-treatment. Together, these findings suggest that the failure of crizotinib to inhibit the downstream pathways utilized by ALK^{F1174L} and MYCN can be overcome by adding an effective downstream pathway inhibitor, such as Torin2.

DISCUSSION

Activating mutations in the ALK receptor tyrosine kinase represent potentially useful therapeutic targets in high-risk neuroblastoma. In contrast to MYCN, which has been difficult to target (Gustafson and Weiss, 2010), mutated ALK lends itself to inhibition by small molecules and hence may spawn a generation of targeted therapies for this resistant tumor. Here we used a mouse model of neuroblastoma coexpressing *ALK*^{F1174L} and *MYCN* to demonstrate that constitutive ALK^{F1174L} activity potentiates the oncogenic effects of MYCN, resulting in the formation of aggressive, highly penetrant tumors. Similar cooperativity between ALK^{F1174L} and MYCN was recently observed in a zebrafish

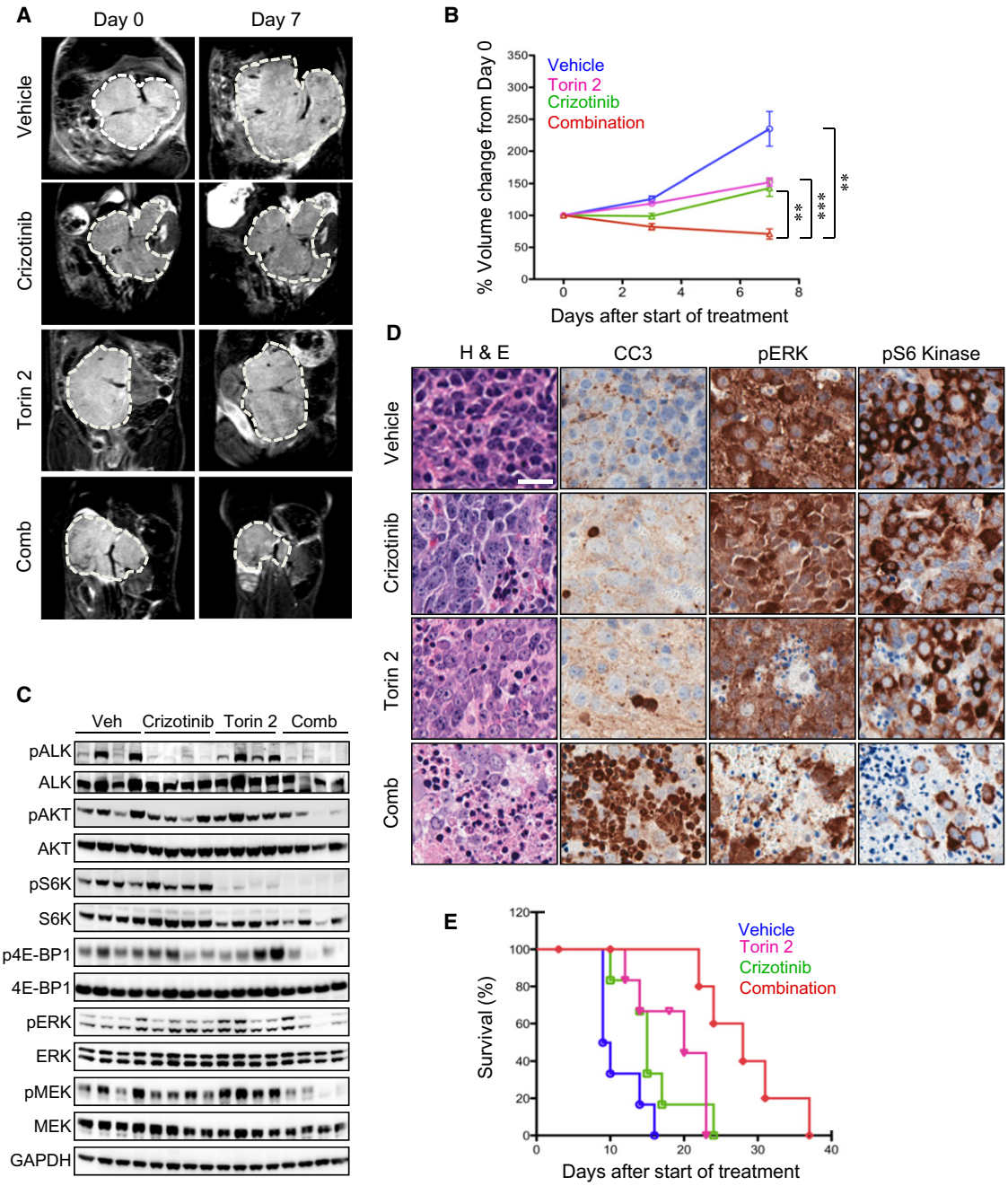

Figure 7. Combined Targeting of ALK^{F1174L} and mTOR Is Effective against ALK^{F1174L}/*MYCN* Neuroblastomas

(A) MRI images depicting a representative tumor response to vehicle or crizotinib (100 mg/kg) and Torin2 (20 mg/kg) as single agents or in combination (at single agent doses) after 7 days of treatment. Comb, combination treatment.

(B) Quantitation of changes in tumor volume in animals treated with crizotinib, Torin2, or combination therapy as measured by MRI on days 0, 3 and 7. Data are presented as means ± SEM (4 animals per treatment group). Crizotinib versus combination, **p = 0.003; Torin2 versus combination; ***p = 0.0002; vehicle versus combination, **p = 0.002; all by Student's t test.

(C) Western blot analysis of the indicated proteins in ALK^{F1174L}/*MYCN* tumors in panels (A) and (B). Veh, vehicle; Comb, combination.

(D) H&E and immunohistochemical staining of tumors in (A) and (B) as indicated. Comb, combination treatment. Scale bars, 10 μm.

(E) Kaplan-Meier survival analysis for ALK^{F1174L}/*MYCN* animals (10 per group) treated for 14 days with crizotinib and Torin2 as single or combined agents. Crizotinib versus combination, p = 0.007; Torin2 versus combination, p = 0.02; both comparisons by log-rank test.

See also Figure S5 and Table S1.

model (Zhu et al., 2012). The acceleration of tumorigenesis by mutant ALK is accompanied by activation of signaling pathways that lead to stabilization of the MYCN protein while countering its pro-apoptotic effects. We also show that our *ALK*^{F1174L}/*MYCN* tumor model recapitulates the in vitro resistance of ALK^{F1174L}–positive tumor cells to crizotinib, but that the combination of crizotinib and an mTOR inhibitor, Torin2, can circumvent this resistance, leading to marked tumor regression and prolongation of survival.

ALK^{F1174L}, although shown to be transforming in NIH 3T3 and Ba/F3 assays (Chen et al., 2008; De Brouwer et al., 2010; George et al., 2008; Janoueix-Lerosey et al., 2008), did not appear to be sufficient by itself to induce tumors in our model. The reasons underlying this are not entirely clear, but given the fact that *ALK* mutations have been identified in both high- and low-stage tumors, it is conceivable that while activated ALK has a role in tumor initiation, cooperation with additional aberrations such as *MYCN* amplification or loss of tumor suppressors on chromosome 1p or 11q are required to specify high- versus low-stage tumors. Serial analysis of developing sympathetic tissues from *Th-ALK*^{F1174L} mice will be useful in determining whether neuroblast cell hyperplasia or even localized tumors develop in these animals, which then regress in the absence of cooperative genetic events.

Of interest, the *ALK*^{F1174L} mutation has not been reported in the germline of patients with familial neuroblastoma. This could indicate that either high levels of activated ALK kinase activity or functions specific to the ALK^{F1174L} mutation are not tolerated during embryogenesis. By contrast, we observed Mendelian distribution of *ALK*^{F1174L} alleles in crosses of our *Th-ALK*^{F1174L} animals suggesting absence of embryonic lethality. The approach we used to generate our murine model does not modify the endogenous *ALK* alleles and therefore the developmentally essential expression of endogenous *ALK* in the CNS and other organs (Vernersson et al., 2006) presumably remains unaltered. Moreover, the *Th*-driven *ALK*^{F1174L} mutation exhibits tissue-specific expression in relatively more differentiated *Th*-positive sympathetic neuronal precursors. To more accurately address these issues, a knock-in modeling strategy replacing an endogenous *Alk* allele with an inducible *ALK*^{F1174L} allele would be required.

In the *Th-MYCN* model, heterozygote animals of the 129X1/SvJ strain develop neuroblastoma within 4 to 5 months accompanied by additional chromosomal gains or losses, whereas homozygous animals show increased penetrance and shorter latency of tumors that approaches 100% at three months, without the requirement for additional chromosomal lesions (Weiss et al., 1997). Thus, a small increase in MYCN dosage is sufficient to augment MYCN-driven tumorigenesis. We observed increased MYCN protein stability in *ALK*^{F1174L}/*MYCN* transgenic tumors. MYCN stability is specifically regulated by sequential phosphorylation of S62 and T58 within MYC Box 1, the former through either CDK1 or the MAPK pathway (Marshall et al., 2011; Sears et al., 2000; Sjostrom et al., 2005), and the latter, through the PI3K/AKT pathway via GSK3β-mediated inhibitory phosphorylation (Sears et al., 2000). AKT- or ERK-mediated mTORC1 signaling also downregulates PP2A, which normally dephosphorylates MYCN at S62, targeting pMYCN^{T58} for ubiquitination and degradation by the E3 ligase FBXW7 (Gustafson and Weiss, 2010). We demonstrate that increased activation of the PI3K/AKT/mTOR pathway and additional recruitment of the MAPK pathway combine to stabilize MYCN in *ALK*^{F1174L}/*MYCN* tumors. We suggest that the discrepancy between MYCN levels on immunohistochemical staining versus immunoblotting reflects the very short half-life and high rate of synthesis of this oncoprotein in vivo. *Th-MYCN* tumors have very high levels of MYCN protein even in the absence of ALK expression (Weiss et al., 1997), and the limited dynamic range of immunoblotting may hinder the detection of increased total MYCN by this method.

We also report that the stabilization of the MYCN protein seen in *ALK*^{F1174L}/*MYCN* tumors is augmented by increased levels of endogenous *Mycn* transcripts, confirming recent in vitro findings that both WT and gain of function *ALK* mutations stimulate *MYCN* transcription (Schönherr et al., 2012). The mechanism underlying this phenomenon is unclear, but could be due to either an indirect effect of ALK^{F1174L} signaling on the *Mycn* promoter (Wierstra and Alves, 2008) or loss of *Mycn* autorepression. Indeed, as reported by Penn et al. (Penn et al., 1990), MYC suppresses transcription from its own promoter when the level of the oncoprotein exceeds 10,000 molecules per cell. It seems reasonable, then, to suggest that signaling mediated by ALK^{F1174L} either prevents or abolishes a block at the *Mycn* promoter, allowing unimpeded gene transcription. Such ALK^{F1174L}-induced regulation of Mycn could occur during early development, leading to sustained high levels of MYCN in sympathetic neuronal precursor cells, which then sets the stage for rapid malignant transformation.

The relative lack of apoptosis in our tumor model suggests that ALK^{F1174L} counteracts MYCN-induced cell death as part of the transformed phenotype. We noted significant downregulation of the pro-apoptotic BCL2 proteins NOXA, BID, and BAX, all transcriptional targets of p53, which itself was downregulated in the *ALK*^{F1174L}/*MYCN* tumors. Accompanying these findings was upregulation of the anti-apoptotic BCLW and, to a lesser extent, BCL2 proteins. The upregulation of BCLW is particularly relevant because it has been shown to counteract apoptosis induced by nerve growth factor deprivation and BAD overexpression in sympathetic neuronal cells (Hamnér et al., 2001). Moreover, the overexpression of BCLW and BCL2, but not MCL1, places the *ALK*^{F1174L}/*MYCN* tumors in the subset of neuroblastomas that are predicted to be sensitive to the BCL2 inhibitor ABT-737 (Goldsmith et al., 2010), thus providing an additional avenue for therapeutic targeting of these tumors. In other receptor tyrosine kinase-activated cancers and in tumors positive for ALK fusion proteins, resistance to apoptosis is mediated through signal transduction pathways that directly enhance the transcription of anti-apoptotic factors such as *BCLXL* while inhibiting pro-apoptotic genes (Chiarle et al., 2008). We therefore suggest that the anti-apoptotic effect seen in *ALK*^{F1174L}/*MYCN* tumors arises from ALK^{F1174L}-mediated activation of both the PI3K/AKT/mTOR and MAPK signaling cascades.

The demonstration that *ALK* cooperates with *MYCN* to accelerate tumorigenesis helps to explain the role of oncogenes such as *MYCN* during tumor initiation. The bulk of evidence suggests that MYC oncoproteins play a critical role during this phase of tumor development, where high levels are required to initiate and expand oncogenic clones (Arvanitis and Felsher, 2006;

Soucek and Evan, 2010), usually in combination with an apoptotic defect (Hansford et al., 2004). We propose that activated *ALK* simultaneously stabilizes MYCN protein and uncouples MYCN-driven apoptosis, potentiating the oncogenic activity of MYCN during early development of neuroblasts. This concept is also relevant to the clinical observation that prognosis in neuroblastoma is strongly associated with *MYCN* gene copy number but only variably with protein levels (Cohn et al., 2000). In contrast to the situation during tumor initiation, low, "threshold" levels of MYC are likely sufficient to maintain progression of oncogene-addicted, established tumors, and prevent the switch from ongoing proliferation to apoptosis/necrosis (Murphy et al., 2008; Shachaf et al., 2008). Therefore, stabilization of MYCN by modulation of MYC Box 1 phosphorylation (Marshall et al., 2011) or inhibition of MYCN protein ubiquitination and degradation (Otto et al., 2009) are both mechanisms by which stoichiometric control of MYC protein levels are achieved during malignant transformation in precancerous cells (Marshall et al., 2011). Pharmacologic modulation of such pathways that stabilize MYCN abrogates neuroblastoma tumor formation in the *Th-MYCN* model, providing experimental validation of this concept (Chanthery et al., 2012; Marshall et al., 2011).

In MYCN-driven neuroblastoma, the PI3K pathway appears to be the major signaling conduit for regulation of MYCN activity, and selective inhibition of this pathway has been shown to lead to MYCN destabilization and subsequent tumor regression (Chesler et al., 2006). Oncogenic transformation caused by ALK fusion proteins, on the other hand, appears to be effected through several interconnected and overlapping pathways that are differentially recruited by the activated ALK kinase based on cell type, context and fusion partner (Chiarle et al., 2008; Palmer et al., 2009). In anaplastic large cell lymphoma, the aberrant growth of the cells expressing the *NPM-ALK* fusion gene, for example, is mainly attributable to activation of the JAK-STAT and MAPK pathways (Pulford et al., 2004). However, in our tumor model, ALK^{F1174L} utilizes both the PI3K/AKT/mTOR and MAPK pathways to instigate downstream signals leading to increased survival. Interestingly, the same signaling pathways are upregulated when the *F1174L* mutation occurs in the background of *ALK* translocations such as *EML4-ALK* and *RANBP2-ALK* (Heuckmann et al., 2011; Sasaki et al., 2010), suggesting that the same mode of downstream signaling is used whether the mutation arises de novo or as an acquired mechanism of resistance. Hence, the treatment strategy that we propose, in which crizotinib is combined with a downstream pathway inhibitor, may be effective against these cancers, delaying or even preventing the onset of resistance to crizotinib.

For a tyrosine kinase inhibitor to be successful, it must abrogate activity of key intracellular pathways that transmit oncogenic activity of the kinase. We determined that the resistance to crizotinib seen in ALK^{F1174L}/*MYCN*-driven murine neuroblastoma relates to incomplete inhibition of key signaling cascades. Crizotinib treatment, while leading to reduced levels of pALK and pAKT at high doses lacked any effect on pERK or activated mTOR signaling in ALK^{F1174L}/*MYCN* tumors. Thus, in crizotinib-treated animals even a minimal amount of ALK^{F1174L} activity appears sufficient to maintain downstream signaling, especially that of mTORC1. We suggest that both the PI3K/AKT and MAPK pathways contribute to mTORC1 activation in these tumors, but as AKT signaling becomes downregulated by crizotinib, mTORC1 signaling is maintained by the MAPK pathway, which would account for the relative insensitivity of the tumor cells to single agent treatment with Torin2. However, combined treatment with crizotinib and Torin2 induced downregulation of all components of the PI3K/AKT/mTOR as well as MAPK pathways, accompanied by the induction of massive apoptosis. Importantly, suppression of these two signaling pathways, together with ALK^{F1174L} activity, effectively inhibited the growth of ALK^{F1174L}/*MYCN* tumors, leading to significant decreases in tumor volumes and a higher proportion of surviving mice.

Our study indicates that the combination of crizotinib and an ATP-competitive mTOR inhibitor, or perhaps a MEK inhibitor, would afford a useful treatment strategy for neuroblastoma with constitutive activation of ALK^{F1174L} and *MYCN*. The reduced susceptibility of *F1174L*-mutated *ALK* to crizotinib inhibition has been reported to arise from an increased ATP-binding affinity, suggesting that higher doses of crizotinib or substitution of higher-affinity inhibitors may surmount this barrier to successful treatment (Bresler et al., 2011). Although a dose-response relationship to crizotinib as a single agent in ALK^{F1174L}-expressing neuroblastoma cell lines (Bresler et al., 2011; A. Azarova and R.E.G., unpublished data) and in our ALK^{F1174L}/*MYCN* model (L.C. and R.E.G., unpublished data) has been observed, whether the doses of crizotinib required to completely eradicate the tumor will be feasible in a clinical setting remains to be determined. Moreover, prolonged use of even the most effective ALK inhibitor by itself would ultimately generate resistance. Hence, simultaneously attacking more than one vulnerable lesion in neuroblastoma cells seems a more promising strategy to prevent or forestall the development of crizotinib resistance. Indeed, further efficacy might be afforded by the addition of therapeutic agents that inhibit the pro-survival proteins BCL2 and BLCW or that disrupt mechanisms active in the synthesis of MYCN. Regardless of the specific combination of targets, the double transgenic model developed in this study would provide an ideal platform for screening candidate small-molecule inhibitors and elucidating interactions among the aberrant signaling cascades that underlie ALK^{F1174L}/*MYCN*-positive neuroblastoma. Finally, we suggest that simultaneous targeting of ALK and its downstream effector molecules may lengthen the duration of response in a larger group of patients with tumors harboring crizotinib-sensitive ALK. This cohort includes those with other point mutations or amplification of *ALK* as in neuroblastoma, or with *ALK* translocations such as non-small cell lung cancer, inflammatory myofibroblastic tumor, anaplastic large cell lymphoma, and several others.

EXPERIMENTAL PROCEDURES

Plasmids

The ALK^{F1174L} mutation was introduced into WT *ALK* cDNA in pcDNA3.1 (Invitrogen) using the QuickChange II Site-Directed Mutagenesis Kit (Stratagene). All mutations were confirmed by sequencing of the entire *ALK* open reading frame. The ALK^{F1174L} cDNA was ligated downstream of the rat tyrosine hydroxylase (*Th*) promoter (Banerjee et al., 1992) in the *Th-MYCN* transgenic construct after excision of *MYCN* with appropriate restriction enzymes to generate the p4.5 *Th-*ALK^{F1174L} construct. For transient transfections, ALK^{F1174L} was introduced into 293T cells (human embryonic kidney transformed cells) using Fugene 6 transfection reagent (Roche) according to the manufacturer's instructions.

Mouse Models

Th-ALK^{F1174L} founders were derived from *CBA* × *C57BL/6J* mice and genetically crossed with *Th-MYCN* mice of the 129/SvJ strain. Tail DNA of all animals was analyzed for *ALK* and *MYCN* transgenes by qRT-PCR (Transnetyx, Inc.). All animal experiments were conducted in accordance with established UK Home Office guidelines per conditions specified in an animal use authorization license (PPL70-6882) that is approved by The Institute of Cancer Research local ethical review committee.

Tumor Histopathology

Animal tumors were harvested at sacrifice, fixed in 10% neutral buffered formalin, and paraffin-embedded for histologic studies. Tissue sections were stained with H&E and assessed histologically by a pediatric pathologist (A.P.A.) for confirmation of tumor type, and specifically for histologic features of neuroblastoma including amount of stroma and neuropil, mitotic/karyorrhectic index, and degree of differentiation. Representative examples from each of the founder lines were analyzed (*ALK*^{F1174L}/*MYCN* tumors, n = 15; *MYCN* tumors, n = 9). For immunohistochemistry, 5 μm sections were stained with antibodies to ALK (Ventana), MYCN (Calbiochem), pMEK, pS6K, pERK, cleaved caspase 3 (Cell Signaling Technology), and TUNEL (Millipore) using standard methods, including heat-induced epitope retrieval using citrate buffer pH 6 (or EDTA buffer for ALK). Formalin-fixed slides from patients with both ALK^{F1174L}/MYCN-positive and MYCN-positive neuroblastoma tumors were stained using the same antibodies. All human tumor specimens were obtained in accordance with the Institutional Review Boards of Memorial Sloan-Kettering Cancer Center and the Dana-Farber Cancer Institute and deidentified before analysis.

Murine Therapy Trials

Th-MYCN hemizygous mice were bred with *Th-ALK*^{F1174L} hemizygous mice, and litters were genotyped to detect the presence of human *MYCN* or *ALK*^{F1174L} transgenes. After weaning, at about day 28, animals hemizygous for both transgenes or *MYCN* alone were palpated for intra-abdominal tumors twice weekly. Animals with palpable tumors (30–70 days old) were randomized to treatment groups. For intervention trials, mice were treated with 100 mg/kg crizotinib or 20 mg/kg Torin2 as single agents, 100 mg/kg crizotinib and 20 mg/kg Torin2 in combination, or vehicle for 7 days. Crizotinib and Torin2 were administered via oral gavage. MRI was performed on a 7T Bruker horizontal bore microimaging system (Bruker Instruments, Ettlingen, Germany) using a 3-cm birdcage coil. Anatomical T_2-weighted coronal images were acquired from twenty contiguous 1 mm thick slices through the mouse abdomen, from which tumor volumes were determined using segmentation from regions of interest drawn on each tumor-containing slice. At sacrifice, tumors were excised, weighed, snap frozen in liquid nitrogen for metabolic assays, or fixed in 10% neutral buffered formalin. For survival trials, mice were treated with 100 mg/kg crizotinib or 20 mg/kg Torin2 as single agents, 100 mg/kg crizotinib (or 80 mg/kg where indicated) and 20 mg/kg Torin2 in combination, or vehicle for 14 days. Mice were monitored daily; tumor size was palpated and animal weights measured. Animals were sacrificed when pathologic signs of tumor burden (predominantly poor mobility) were apparent.

Statistical Analyses

All biochemical experiments were done in triplicate unless otherwise stated. Two-tailed Student's t test was used to test significance. Survival curves were constructed by the Kaplan and Meier method, with differences between curves tested for statistical significance using the log-rank test; s.d., standard deviation; C.I., confidence interval; s.e.m., standard error of the mean.

ACCESSION NUMBERS

The GEO public database accession number for the microarray data is GSE35560.

SUPPLEMENTAL INFORMATION

Supplemental Information includes five figures, one table, Supplemental Experimental Procedures, and Supplemental References and can be found with the article online at http://dx.doi.org/10.1016/j.ccr.2012.06.001.

ACKNOWLEDGMENTS

We thank Terri Bowman for help with immunohistochemistry. We thank J.R. Gilbert for helpful comments on the manuscript. This work was supported by US National Institutes of Health Grant R01 CA148688 (to R.E.G.), Sidney Kimmel Translational Scholar Award (to R.E.G.), Children's Hospital Boston TRP Pilot Grant (to R.E.G.), NIH Grant CA136851-01A1 (to N.S.G. and Q.L.), the Catie Hoch Foundation and the Robert Steel Foundation (to N.K.C.), SPARKS grant 09RMH01 (to L.C.), Neuroblastoma Society Grant NES003X (to L.C.), Medical Research Council (MRC) Grant NC3R-G1000121/94513 (to L.C. and S.A.E.), ICR and Cancer Research UK (CRUK) Grants A14610 (to L.C.), C309/A8274, and C309/A11566 (to S.A.E.), ICR CRUK/EPSRC/MRC and Department of Health (England) Grant C1060/A10334 (to Y.J. and S.P.R.), CRUK Grant A10294 (to A.D.J.P.), and Wellcome Trust Grant 091763Z/10/Z (to Y.J.). We acknowledge NHS funding to the NIHR Biomedical Research Centre.

Received: January 14, 2012
Revised: March 18, 2012
Accepted: June 5, 2012
Published: July 9, 2012

REFERENCES

Arvanitis, C., and Felsher, D.W. (2006). Conditional transgenic models define how MYC initiates and maintains tumorigenesis. Semin. Cancer Biol. *16*, 313–317.

Banerjee, S.A., Hoppe, P., Brilliant, M., and Chikaraishi, D.M. (1992). 5′ flanking sequences of the rat tyrosine hydroxylase gene target accurate tissue-specific, developmental, and transsynaptic expression in transgenic mice. J. Neurosci. *12*, 4460–4467.

Bresler, S.C., Wood, A.C., Haglund, E.A., Courtright, J., Belcastro, L.T., Plegaria, J.S., Cole, K., Toporovskaya, Y., Zhao, H., Carpenter, E.L., et al. (2011). Differential inhibitor sensitivity of anaplastic lymphoma kinase variants found in neuroblastoma. Sci. Transl. Med. *3*, 108–114.

Brodeur, G.M., Seeger, R.C., Schwab, M., Varmus, H.E., and Bishop, J.M. (1984). Amplification of N-*myc* in untreated human neuroblastomas correlates with advanced disease stage. Science *224*, 1121–1124.

Butrynski, J.E., D'Adamo, D.R., Hornick, J.L., Dal Cin, P., Antonescu, C.R., Jhanwar, S.C., Ladanyi, M., Capelletti, M., Rodig, S.J., Ramaiya, N., et al. (2010). Crizotinib in ALK-rearranged inflammatory myofibroblastic tumor. N. Engl. J. Med. *363*, 1727–1733.

Chanthery, Y.H., Gustafson, W.C., Itsara, M., Persson, A., Hackett, C.S., Grimmer, M., Charron, E., Yakovenko, S., Kim, G., Matthay, K.K., and Weiss, W.A. (2012). Paracrine signaling through MYCN enhances tumor-vascular interactions in neuroblastoma. Sci. Transl. Med. *4*, 115–113.

Chen, Y., Takita, J., Choi, Y.L., Kato, M., Ohira, M., Sanada, M., Wang, L., Soda, M., Kikuchi, A., Igarashi, T., et al. (2008). Oncogenic mutations of ALK kinase in neuroblastoma. Nature *455*, 971–974.

Chesler, L., Schlieve, C., Goldenberg, D.D., Kenney, A., Kim, G., McMillan, A., Matthay, K.K., Rowitch, D., and Weiss, W.A. (2006). Inhibition of phosphatidylinositol 3-kinase destabilizes Mycn protein and blocks malignant progression in neuroblastoma. Cancer Res. *66*, 8139–8146.

Chiarle, R., Voena, C., Ambrogio, C., Piva, R., and Inghirami, G. (2008). The anaplastic lymphoma kinase in the pathogenesis of cancer. Nat. Rev. Cancer *8*, 11–23.

Christensen, J.G., Zou, H.Y., Arango, M.E., Li, Q., Lee, J.H., McDonnell, S.R., Yamazaki, S., Alton, G.R., Mroczkowski, B., and Los, G. (2007). Cytoreductive antitumor activity of PF-2341066, a novel inhibitor of anaplastic lymphoma kinase and c-Met, in experimental models of anaplastic large-cell lymphoma. Mol. Cancer Ther. *6*, 3314–3322.

Cohn, S.L., London, W.B., Huang, D., Katzenstein, H.M., Salwen, H.R., Reinhart, T., Madafiglio, J., Marshall, G.M., Norris, M.D., and Haber, M. (2000). MYCN expression is not prognostic of adverse outcome in advanced-stage neuroblastoma with nonamplified MYCN. J. Clin. Oncol. *18*, 3604–3613.

De Brouwer, S., De Preter, K., Kumps, C., Zabrocki, P., Porcu, M., Westerhout, E.M., Lakeman, A., Vandesompele, J., Hoebeeck, J., Van Maerken, T., et al. (2010). Meta-analysis of neuroblastomas reveals a skewed ALK mutation spectrum in tumors with MYCN amplification. Clin. Cancer Res. *16*, 4353–4362.

George, R.E., Sanda, T., Hanna, M., Fröhling, S., Luther, W., 2nd, Zhang, J., Ahn, Y., Zhou, W., London, W.B., McGrady, P., et al. (2008). Activating mutations in ALK provide a therapeutic target in neuroblastoma. Nature *455*, 975–978.

Goldsmith, K.C., Lestini, B.J., Gross, M., Ip, L., Bhumbla, A., Zhang, X., Zhao, H., Liu, X., and Hogarty, M.D. (2010). BH3 response profiles from neuroblastoma mitochondria predict activity of small molecule Bcl-2 family antagonists. Cell Death Differ. *17*, 872–882.

Gustafson, W.C., and Weiss, W.A. (2010). Myc proteins as therapeutic targets. Oncogene *29*, 1249–1259.

Hamnér, S., Arumäe, U., Li-Ying, Y., Sun, Y.F., Saarma, M., and Lindholm, D. (2001). Functional characterization of two splice variants of rat bad and their interaction with Bcl-w in sympathetic neurons. Mol. Cell. Neurosci. *17*, 97–106.

Hansford, L.M., Thomas, W.D., Keating, J.M., Burkhart, C.A., Peaston, A.E., Norris, M.D., Haber, M., Armati, P.J., Weiss, W.A., and Marshall, G.M. (2004). Mechanisms of embryonal tumor initiation: distinct roles for MycN expression and MYCN amplification. Proc. Natl. Acad. Sci. USA *101*, 12664–12669.

Hemann, M.T., and Lowe, S.W. (2006). The p53-Bcl-2 connection. Cell Death Differ. *13*, 1256–1259.

Heuckmann, J.M., Hölzel, M., Sos, M.L., Heynck, S., Balke-Want, H., Koker, M., Peifer, M., Weiss, J., Lovly, C.M., Grütter, C., et al. (2011). ALK mutations conferring differential resistance to structurally diverse ALK inhibitors. Clin. Cancer Res. *17*, 7394–7401.

Janoueix-Lerosey, I., Lequin, D., Brugières, L., Ribeiro, A., de Pontual, L., Combaret, V., Raynal, V., Puisieux, A., Schleiermacher, G., Pierron, G., et al. (2008). Somatic and germline activating mutations of the ALK kinase receptor in neuroblastoma. Nature *455*, 967–970.

Kwak, E.L., Bang, Y.J., Camidge, D.R., Shaw, A.T., Solomon, B., Maki, R.G., Ou, S.H., Dezube, B.J., Jänne, P.A., Costa, D.B., et al. (2010). Anaplastic lymphoma kinase inhibition in non-small-cell lung cancer. N. Engl. J. Med. *363*, 1693–1703.

Liu, Q., Wang, J., Kang, S.A., Thoreen, C.C., Hur, W., Ahmed, T., Sabatini, D.M., and Gray, N.S. (2011). Discovery of 9-(6-aminopyridin-3-yl)-1-(3-(trifluoromethyl)phenyl)benzo[h][1,6]naphthyridin-2(1H)-one (Torin2) as a potent, selective, and orally available mammalian target of rapamycin (mTOR) inhibitor for treatment of cancer. J. Med. Chem. *54*, 1473–1480.

Marshall, G.M., Liu, P.Y., Gherardi, S., Scarlett, C.J., Bedalov, A., Xu, N., Iraci, N., Valli, E., Ling, D., Thomas, W., et al. (2011). SIRT1 promotes N-Myc oncogenesis through a positive feedback loop involving the effects of MKP3 and ERK on N-Myc protein stability. PLoS Genet. *7*, e1002135.

Matthay, K.K., Villablanca, J.G., Seeger, R.C., Stram, D.O., Harris, R.E., Ramsay, N.K., Swift, P., Shimada, H., Black, C.T., Brodeur, G.M., et al; Children's Cancer Group. (1999). Treatment of high-risk neuroblastoma with intensive chemotherapy, radiotherapy, autologous bone marrow transplantation, and 13-cis-retinoic acid. N. Engl. J. Med. *341*, 1165–1173.

Mossé, Y.P., Laudenslager, M., Longo, L., Cole, K.A., Wood, A., Attiyeh, E.F., Laquaglia, M.J., Sennett, R., Lynch, J.E., Perri, P., et al. (2008). Identification of ALK as a major familial neuroblastoma predisposition gene. Nature *455*, 930–935.

Murphy, D.J., Junttila, M.R., Pouyet, L., Karnezis, A., Shchors, K., Bui, D.A., Brown-Swigart, L., Johnson, L., and Evan, G.I. (2008). Distinct thresholds govern Myc's biological output in vivo. Cancer Cell *14*, 447–457.

Otto, T., Horn, S., Brockmann, M., Eilers, U., Schüttrumpf, L., Popov, N., Kenney, A.M., Schulte, J.H., Beijersbergen, R., Christiansen, H., et al. (2009). Stabilization of N-Myc is a critical function of Aurora A in human neuroblastoma. Cancer Cell *15*, 67–78.

National Cancer Institute. (2005). Surveillance, Epidemiology and End Results Database. http://seer.cancer.gov/publications/childhood/sympathetic.pdf.

Palmer, R.H., Vernersson, E., Grabbe, C., and Hallberg, B. (2009). Anaplastic lymphoma kinase: signalling in development and disease. Biochem. J. *420*, 345–361.

Pelengaris, S., Khan, M., and Evan, G. (2002). c-MYC: more than just a matter of life and death. Nat. Rev. Cancer *2*, 764–776.

Penn, L.J., Brooks, M.W., Laufer, E.M., and Land, H. (1990). Negative autoregulation of c-myc transcription. EMBO J. *9*, 1113–1121.

Pulford, K., Morris, S.W., and Turturro, F. (2004). Anaplastic lymphoma kinase proteins in growth control and cancer. J. Cell. Physiol. *199*, 330–358.

Sasaki, T., Okuda, K., Zheng, W., Butrynski, J., Capelletti, M., Wang, L., Gray, N.S., Wilner, K., Christensen, J.G., Demetri, G., et al. (2010). The neuroblastoma-associated F1174L ALK mutation causes resistance to an ALK kinase inhibitor in ALK-translocated cancers. Cancer Res. *70*, 10038–10043.

Schönherr, C., Ruuth, K., Kamaraj, S., Wang, C.L., Yang, H.L., Combaret, V., Djos, A., Martinsson, T., Christensen, J.G., Palmer, R.H., and Hallberg, B. (2012). Anaplastic lymphoma kinase (ALK) regulates initiation of transcription of MYCN in neuroblastoma cells. Oncogene, Jan 30. [Epub ahead of print].

Schwab, M., Varmus, H.E., Bishop, J.M., Grzeschik, K.H., Naylor, S.L., Sakaguchi, A.Y., Brodeur, G., and Trent, J. (1984). Chromosome localization in normal human cells and neuroblastomas of a gene related to c-myc. Nature *308*, 288–291.

Sears, R., Nuckolls, F., Haura, E., Taya, Y., Tamai, K., and Nevins, J.R. (2000). Multiple Ras-dependent phosphorylation pathways regulate Myc protein stability. Genes Dev. *14*, 2501–2514.

Seeger, R.C., Brodeur, G.M., Sather, H., Dalton, A., Siegel, S.E., Wong, K.Y., and Hammond, D. (1985). Association of multiple copies of the N-myc oncogene with rapid progression of neuroblastomas. N. Engl. J. Med. *313*, 1111–1116.

Shachaf, C.M., Gentles, A.J., Elchuri, S., Sahoo, D., Soen, Y., Sharpe, O., Perez, O.D., Chang, M., Mitchel, D., Robinson, W.H., et al. (2008). Genomic and proteomic analysis reveals a threshold level of MYC required for tumor maintenance. Cancer Res. *68*, 5132–5142.

Sjostrom, S.K., Finn, G., Hahn, W.C., Rowitch, D.H., and Kenney, A.M. (2005). The Cdk1 complex plays a prime role in regulating N-myc phosphorylation and turnover in neural precursors. Dev. Cell *9*, 327–338.

Soucek, L., and Evan, G.I. (2010). The ups and downs of Myc biology. Curr. Opin. Genet. Dev. *20*, 91–95.

Vernersson, E., Khoo, N.K., Henriksson, M.L., Roos, G., Palmer, R.H., and Hallberg, B. (2006). Characterization of the expression of the ALK receptor tyrosine kinase in mice. Gene Expr. Patterns *6*, 448–461.

Weiss, W.A., Aldape, K., Mohapatra, G., Feuerstein, B.G., and Bishop, J.M. (1997). Targeted expression of MYCN causes neuroblastoma in transgenic mice. EMBO J. *16*, 2985–2995.

Wierstra, I., and Alves, J. (2008). The c-myc promoter: still MysterY and challenge. Adv. Cancer Res. *99*, 113–333.

Zhu, S., Lee, J.S., Guo, F., Shin, J., Perez-Atayde, A.R., Kutok, J.L., Rodig, S.J., Neuberg, D.S., Helman, D., Feng, H., et al. (2012). Activated ALK collaborates with MYCN in neuroblastoma pathogenesis. Cancer Cell *21*, 362–373.